CHEMISTRY OF MATERIALS

ARTICLE

pubs.acs.org/cm

Controlling the Microstructure of Solution-Processable Small Molecules in Thin-Film Transistors through Substrate Chemistry

R. Joseph Kline,*[,†] Steven D. Hudson,[†] Xinran Zhang,[†] David J. Gundlach,[‡] Andrew J. Moad,[§] Oana D. Jurchescu,[∥] Thomas N. Jackson,[⊥] Sankar Subramanian,[#] John E. Anthony,[#] Michael F. Toney,[○] and Lee J. Richter*[,§]

[†]Polymers Division, [‡]Semiconductor Electronics Division, and [§]Surface and Microanalysis Science Division, National Institute of Standards and Technology, Gaithersburg, Maryland 20899-1070, United States

[∥]Department of Physics, Wake Forest University, Winston-Salem, North Carolina 27106, United States

[⊥]Center for Thin Film Devices and Materials Research Institute, Department of Electrical Engineering, Penn State University, University Park, Pennsylvania 16802, United States

[#]Department of Chemistry, University of Kentucky, Lexington, Kentucky 40506, United States

[○]Stanford Synchrotron Radiation Lightsource, Menlo Park, California 94025, United States

Supporting Information

ABSTRACT: Solution-processable small molecules have tremendous potential in macroelectronics applications by providing both high charge carrier mobility and low cost processing. Fluorinated 5,11-bis(triethylsilylethynl) anthradithiophene enables high performance thin film transistors due, in part, to a self-patterning process where crystals grow from chemically tailored contacts and bridge the transistor channel. This paper outlines a detailed microstructural study that identifies the crystallization mechanisms of the self-patterning. Two crystal habits are observed: we find that crystals on chemically modified electrodes predominantly form (001) oriented platelets while untreated surfaces form a fine mixture of (001) and (111) oriented crystals. For (001) oriented platelets, the (010) fast growth face lies in the plane of the film and allows extended growth from platelets nucleated on the electrode into the transistor channel. The in-plane charge carrier mobility of the (001) platelets is high; for short channel lengths, crystal growth fronts from adjacent electrodes bridge the channel gap, resulting in the excellent device performance. On untreated surfaces between devices, the low charge carrier mobility, finely mixed state provides self-isolation for stable device operation.

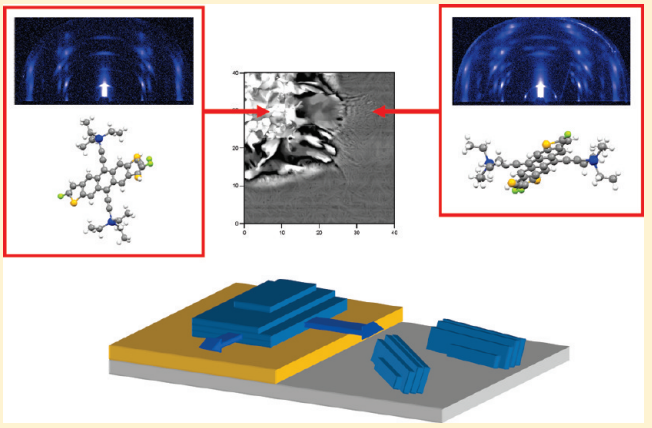

KEYWORDS: organic electronics, thin-film transistors, grazing-incidence X-ray diffraction, transmission electron microscopy, FTIR, TESADT, crystal habits, morphology

INTRODUCTION

The production of thin-film transistors (TFTs) by low-cost methods such as roll-to-roll processing and printing promises to be a disruptive technology, enabling item level RFID tags, flexible displays, and many other unique products.[1−3] Much interest has been invested in correlating the physical structure and electrical characteristics of devices based on thin films of organic molecules. The synthetic diversity presented by organic molecules facilitates the inexpensive patterning and low temperature processing necessary for macroelectronics commercialization. In general, the highest performance has been achieved with small, polycyclic aromatic molecules such as pentacene and rubrene where both single crystal[4−9] and evaporated thin film[10−12] devices can achieve charge-carrier mobilities in excess of 5 $cm^2/(V\,s)$. The high performance has been related to the high level of crystalline order in the thin films. Alternatively, the solution processability required for printing of devices has primarily been limited to semiconducting polymers with generally lower performance, attributed to a lower level of structural order.[13−15]

Solubility can be conferred to small molecules by the addition of appropriate side groups,[16] or by using thermally or photolytically convertable soluble precursors.[17,18] Silylethyne substitution of acenes has emerged as a promising synthetic paradigm for

Received: September 30, 2010
Revised: January 7, 2011
Published: February 04, 2011

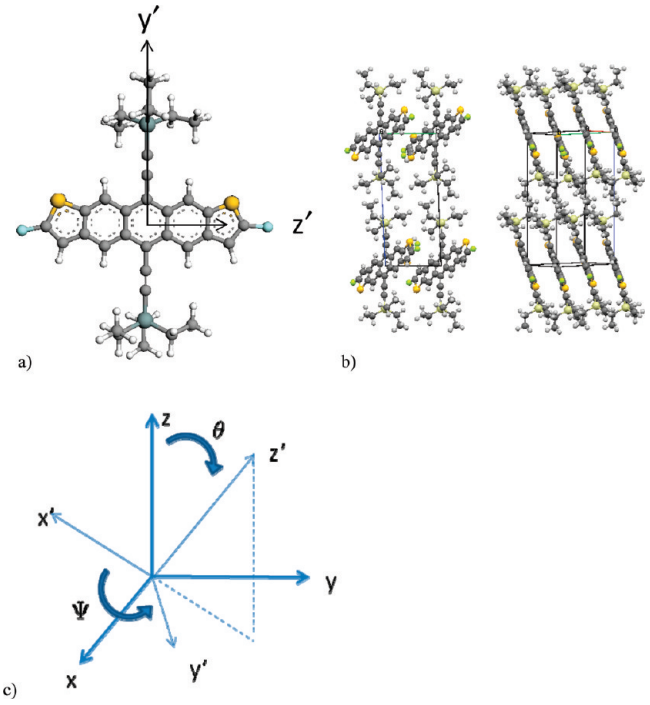

Figure 1. (a) Molecular structure of the syn form of diF-TESADT. (b) Triclinic crystal structure of the high temperature phase of diF-TESADT.[31] (c) Definition of Euler rotation angles θ (tilt from surface normal) and ψ (twist about z′) between the molecular frame (see a) and lab frame. Molecules with the fused core long axis oriented in the transport plane will have $\theta \approx 90°$; those with edge-on orientation will have $\Psi \approx 90°$.

design of optimal, solution processable material.[19] The introduction of the silylethyne side groups allows rational engineering of the crystal packing such as inhibiting the typical herringbone structure of planar aromatic systems and promoting cofacial interactions.[16] Substitution can also confer chemical stability, as the more reactive sites on the molecule can be passivated by the side group. Small molecule blends with polymers have also been used to optimize the charge transport and processability.[20,21]

Shown in Figure 1a is the molecular structure of fluorinated 5,11-bis(triethylsilylethynyl) anthradithiophene (diF-TESADT). Thin films of the unfluorinated analogue, TESADT, are typically amorphous when spin-coated and require post-processing such as solvent annealing[22] or the addition of small amounts diF-TESADT[23] to develop adequate order to support high performance TFTs. Fluorination of the chromophore improves the crystal formation characteristics and confers oxidative stability by lowering the highest occupied molecular orbital (HOMO).[24,25] The strong tendency to crystal formation in diF-TESADT results in polycrystalline films even under the rapid drying conditions of spin-coating.[26−28] It has been found that proper chemical treatment of the device contacts leads to beneficial self-patterning where crystals nucleate on the contacts and extend into the channel of the TFT.[26,29] The highest mobilities are obtained for short channel devices where the contact-nucleated crystals bridge the channel. The self-patterning enables thin film performance that approaches the mobility of single crystal devices with minimal processing.[6,30]

In this report, we present detailed structural characterization of thin films of diF-TESADT spin coated onto a variety of treated and untreated Au and SiO_2 surfaces that model device source-drain contacts and channels. Using X-ray diffraction, polarized infrared spectroscopy, and optical, electron, and atomic force microscopies we identify the specific film crystal structures, orientations, and growth models. In particular, the investigation of the local morphology, the variation of the film structure and crystallite orientation with surface treatment, provides fundamental insights into the practical control of the development of order in this system.

EXPERIMENTAL METHODS

A 50−50 inseparable mixture of the *syn-* and *anti-* forms of diF-TESADT (figure 1) was prepared by a previously reported synthesis.[25] All films were prepared by spin-coating from a chlorobenzene solution (2% by mass) at 1000 rpm ($1000 \times 2\pi$ rad min^{-1}) unless otherwise noted. The typical film thickness was ≈55 nm as measured by spectroscopic ellipsometry. The final stages of film formation during drying took a few seconds.

Transport measurements were made on TFTs in a bottom contact, bottom gate configuration. The gate dielectric was nominally 200 nm of SiO_2 on a highly doped (0.05 Ω-cm), p-type Si wafer. The Si wafer served as both substrate and gate electrode. The source/drain contacts were ≈40 nm of Au on ≈5 nm of Ti, patterned by conventional lift-off processing. The channels were 1 mm wide with lengths varying from (5 to 100) μm. The TFT substrates were cleaned with acetone and isopropanol followed by a UV ozone treatment and deionized water rinse prior to further processing. Prior to deposition of the semiconductor, the contacts were treated via solution deposition of thiols [benzene thiol (BT), perfluorinated benzene thiol (PFBT), or perchlorinated benzene thiol (PClBT)] from ethanol solutions. The mobilities were calculated in the saturation regime. Blanket film structural characterization was performed on films spin coated onto either Si wafers (native oxide) or vapor-deposited Au films (≈100 nm on Si wafers, Platypus Technologies[32]) cleaned via acetone and isopropanol followed by a UV ozone treatment and deionized water rinse. The thiol monolayers for both TFT electrode treatment and blanket film studies were deposited by soaking the substrate in a 100 mmol/L room-temperature solution in ethanol for 30 min, followed by thorough ethanol rinse. The resultant monolayers were characterized by contact angle, ellipsometry, IR spectroscopy, and X-ray photoelectron spectroscopy (XPS). On the basis of XPS, the surface coverage is between (2 to 3) $\times$ 10^{14} cm^{-2}. Details are provided in the Supporting Information.

Grazing incidence X-ray diffraction (GIXD) spectra were collected at the Stanford Synchrotron Radiation Lightsource (SSRL) Beamline 11−3 with an X-ray wavelength of 0.9752 Å, an incidence angle of 0.12°, and an area detector (MAR345).[33] The incidence angle was chosen to be greater than the critical angle of the film but less than the critical angle of the substrate so that the measurement sampled the entire film thickness, but minimized the contribution from the substrate. The measurement was calibrated using a LaB_6 standard. Atomic force microscopy (AFM) was performed with an Asylum Research MFP-3D in resonant mode using Nanosensor probes (PPP-NCL).

A Philips EM400T transmission electron microscope (TEM), operated at 120 kV was used to perform electron imaging and diffraction. The images were recorded with an SIS Cantega 2K CCD camera. For TEM specimen preparation, a thin layer of carbon was evaporated onto the sample, either a blanket film or a diF-TESADT-covered TFT substrate. Poly(acrylic acid) (PAA) aqueous solution (20% by mass) was then drop-cast on top of the film. After drying overnight at 55 °C, the solidified PAA disk, along with the film underneath, was detached from the substrate. The film was picked up by a blank copper grid after PAA was dissolved by floating the disk on water for ≈3 h. The retrieved film was washed repetitively by touching the back side of the copper grid to clean drops of water and then to a filter paper edge.

DiF-TESADT thin films on double side polished SiO_2 (native oxide) wafers were characterized by polarized IR spectroscopy at Brewster's

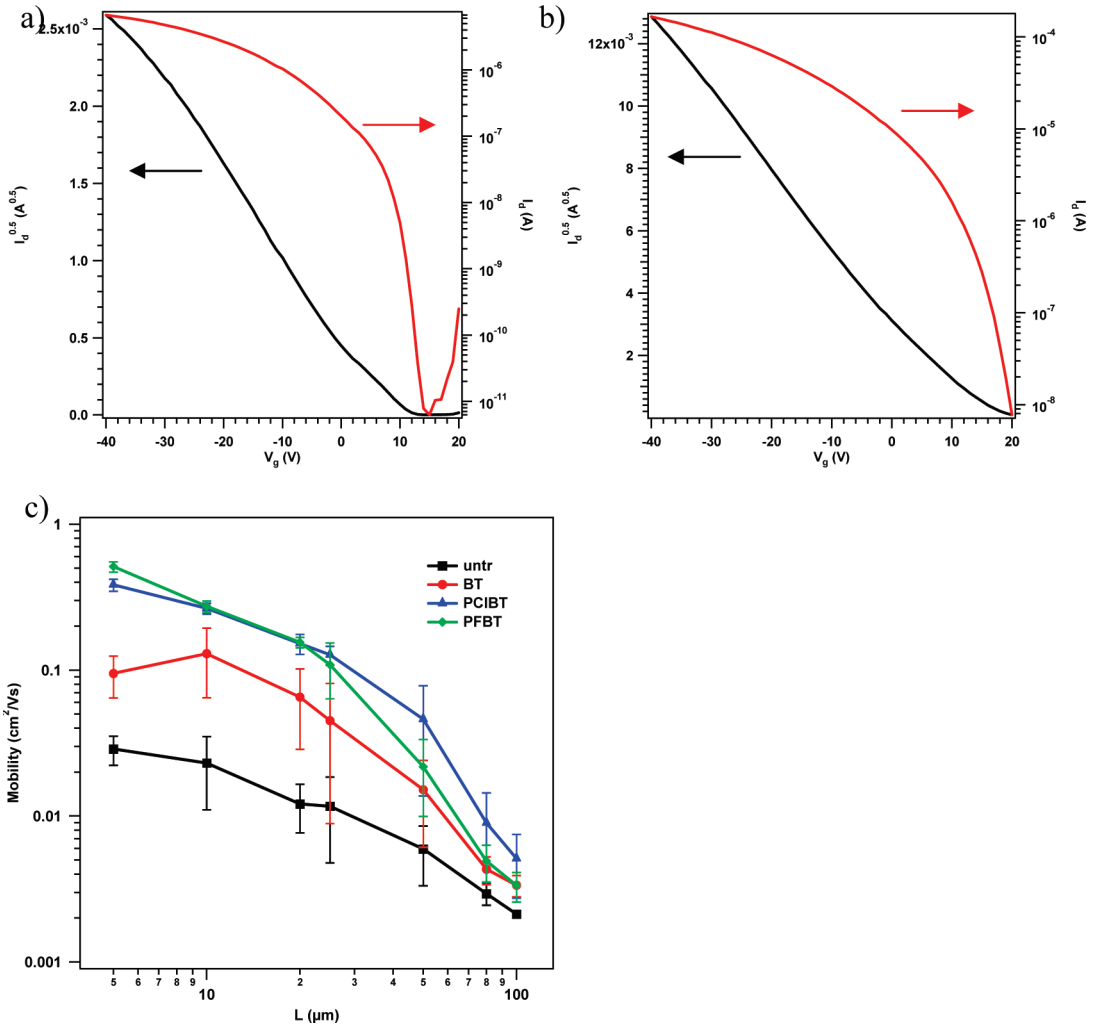

Figure 2. (a) Right axis: transfer characteristics ($I_D - V_{GS}$) for a diF-TESADT TFT with PFBT-treated contacts and $L = 20\ \mu$m and $W = 1000\ \mu$m, at $V_{DS} = -40$ V. Left axis: $\sqrt{I_D} - V_{GS}$ plot in the saturation regime. The extracted saturation mobility is 0.14 $cm^2/(Vs)$ and $V_T = 5$ V. (b) Similar results for a diF-TESADT TFT with untreated contacts with $W = 500\ \mu$m. The extracted saturation mobility is 0.01 $cm^2/(Vs)$ and $V_T = 5$ V. (c) Plot of saturation mobility versus channel length for various surface treatments.

angle (73.7°) employing a custom variable-angle goniometer. Both *s* (electric field vector perpendicular to the plane of incidence) and *p* (electric field vector in the plane of incidence) polarized transmission spectra were recorded using a wire grid polarizer. The spectra were quantified by a nonlinear least-squares fit to multiple Lorentzian lines.[34] DiF-TESADT films and thiol monolayers deposited on Au were characterized with *p*-polarized (wire grid polarizer) reflection absorption infrared spectroscopy (RAIRS) employing a commercial 75° angle-of-incidence grazing reflection accessory. Further experimental details can be found in previous publications.[35] Uncertainties were calculated as an estimated standard deviation from the mean based on independent film preparations.

RESULTS

TFTs with various Au electrode surface treatments were fabricated and electrically tested. Figure 2 shows typical electrical properties for transistors with PFBT-treated and untreated electrodes. The transfer characteristics are excellent, with slight curvature of $\sqrt{I_d}$ versus V_g at low voltage suggestive of contact effects, possibly because of the low HOMO. The saturation mobility μ was extracted from the clear linear region of $\sqrt{I_d}$ versus V_g. Figure 2c shows a plot of the μ versus channel length for various electrode treatments. The charge carrier mobility increased with decreasing channel length for all treatments, with the rate of increase being much higher for treated-contacts and mobilities in excess of 0.5 $cm^2/(V\ s)$ were obtained for 5 μm channel lengths. For 100 μm channel lengths, the mobility of treated electrodes was about 2 times higher than untreated, while at short channel lengths (<20 μm) the mobilities were 10 to 20 times higher with treatment, although greater differences have been reported.[20] The mobilities were found to be similar for both PFBT and PClBT-treated electrodes. BT-treated electrodes were intermediate between PFBT and untreated electrodes. For the structural studies we will emphasize the PFBT-treated electrodes, but similar results were obtained for PClBT-treated electrodes.

Blanket Films. Figure 3 shows 2D-GIXD measurements comparing thin films of DiF-TESADT spin coated onto PFBT-treated Au and bare oxide terminated substrates. DiF-TESADT exhibits at least 2 reversible polymorphs in the bulk with a transition temperature of 294 K.[31] Both are triclinic with space group $P\bar{1}$. In both polymorphs, the ADT cores π-stack in approximately the *a*-*b* plane with the side groups oriented nominally along the *c* axis in a lamella-like structure as shown in

dx.doi.org/10.1021/cm102834m |*Chem. Mater.* 2011, 23, 1194–1203

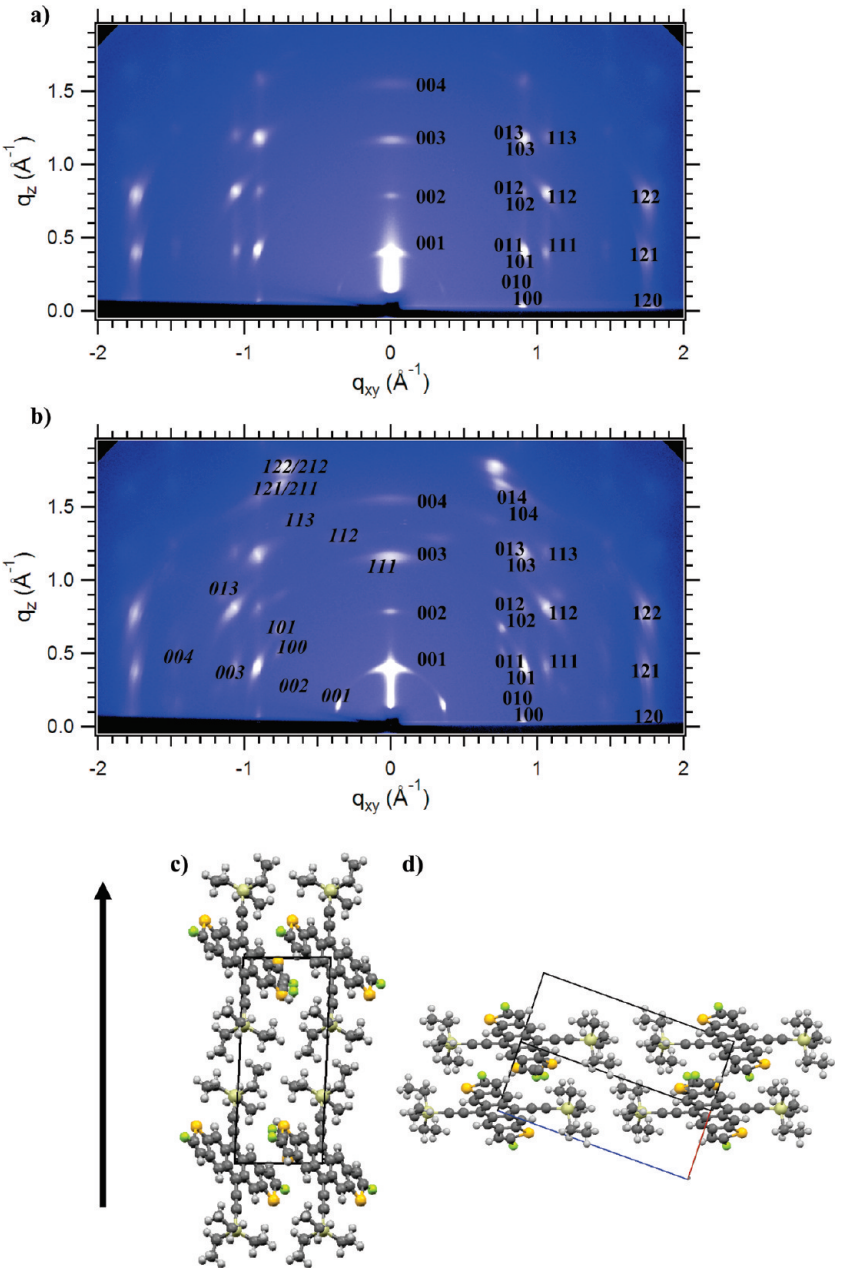

Figure 3. GIXD of blanket films of DiF-TESADT on (a) PFBT-treated Au and (b) untreated oxide. Indices on right denote the peaks of the (001) orientation while italicized indices on left denote the peaks corresponding to the crystals with (111) orientation. A significant amount of (111) oriented crystals are present on the untreated oxide, while only a small amounts of the (111) orientation are present in the PFBT-treated diffraction pattern. The molecular orientations corresponding to these unit cell orientations are shown for the (c) (001) and (d) (111) orientations. The arrow indicates the substrate normal and the box denotes the unit cell.

Figure 1. DiF-TESADT films on PFBT-treated Au are highly crystalline with the crystals predominantly oriented with the (001) orientation normal to the substrate (Figure 3c). This orientation has the π-planes of the molecules and the long-axis of the conjugated core oriented approximately in the plane of the film and is expected to be the optimal orientation for TFT charge transport. Transport measurements on single crystals with (001) orientation have reported mobilities as high as 5 $cm^2 V^{-1} s^{-1}$.[6] The polycrystalline films have a random in-plane orientation within the beam footprint of 150 μm by 10 mm with the diffraction pattern being consistent with a film with large crystals. The unit cell for the single-crystal high-temperature polymorph (**a** = 7.21 Å, **b** = 7.32 Å, **c** = 16.35 Å, α = 87.72°, β = 89.99°, γ = 71.94°) fits the thin-film diffraction reasonably well, indicating that no distinct thin-film phase is present in DiF-TESADT.[6,31] DiF-TESADT films on untreated oxide have diffraction peaks in addition to those of (001) oriented crystals. These additional peaks have significant intensity and can be indexed to (111) oriented crystals with nominally the same unit cell as the (001) crystals. The (111) orientation has the π-planes lying flat (parallel) on the substrate surface as shown in Figure 3d and is expected to be deleterious to charge transport along the TFT channel. Nevertheless this orientation in the field outside of devices provides an electrically insulating boundary to isolate neighboring

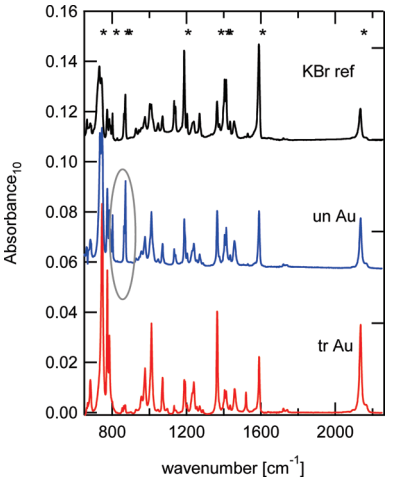

Figure 4. IR spectra: top, diF-TESADT in a KBr disk; middle, RAIRS for a film deposited on untreated Au; bottom, RAIRS for a film deposited on PFBT-treated Au. The asterisks denote those lines used for the orientation analysis. Highlighted are the C═C−H wagging modes, absent in the spectra from tr Au.

devices.[26] Nearly identical diffraction patterns with a mixture of (001) and (111) orientations were also obtained on untreated Au, indicating the presence of the polarizable metal surface, and the corresponding increase in surface roughness has a minimal effect on the crystal structure, preferred orientation, and film formation of DiF-TESADT. We note that small amounts of the (111) orientation are occasionally observed in the diffraction from films on PFBT-treated substrates and are likely due to isolated, non-representative regions within the large sampling area of the measurement.

Unlike GIXD, which is only sensitive to the crystalline regions of the film, FTIR samples the entire film, both ordered and disordered regions and thus is a useful complement. Because of the ≈180° phase shift upon reflection from a metal for s-polarized (electric field vector parallel to the surface) light, the electric field is essentially only along the surface normal. This gives rise to the surface selection rule: only vibrations with an IR transition dipole moment with a component along the surface normal are observed in RAIRS. For a system with C_{2v} symmetry, the dielectric function is diagonal, and all IR active transitions must lie along one of the three eigen axes of the system (x', y', z' in Figure 1). In this case, the average of the Euler angles θ and ψ (see Figure 1) defining the orientation of the molecule in the surface coordinate system of an azimuthally isotropic film ($\langle\cos^2\theta\rangle$ and $\langle\cos^2\Psi\rangle$) can be determined from comparison of the absorption lines in the RAIRS to that of an isotropic reference, typically a KBr pellet.[36] Shown in Figure 4 are IR absorbance spectra for diF-TESADT dispersed in a pressed KBr pellet, and RAIR spectra for diF-TESADT on PFBT treated and untreated Au. From Figure 4, it is clear that the relative intensities of the transitions are different between the RAIR spectra and the pellet, indicating that the films are not isotropic, and are different between PFBT-treated Au and untreated Au. While the core of the *syn* isomer of the isolated molecule is C_{2v}, that of the *anti* is C_{2h} and modes in the y'-z' plane can have mixed dipole orientations. Additionally, intermolecule coupling in the low symmetry (triclinic) crystal can alter the eigen-axes of the crystal dielectric tensor with respect to the molecule. We have performed density functional theory calculations to both assign the vibrational spectrum and

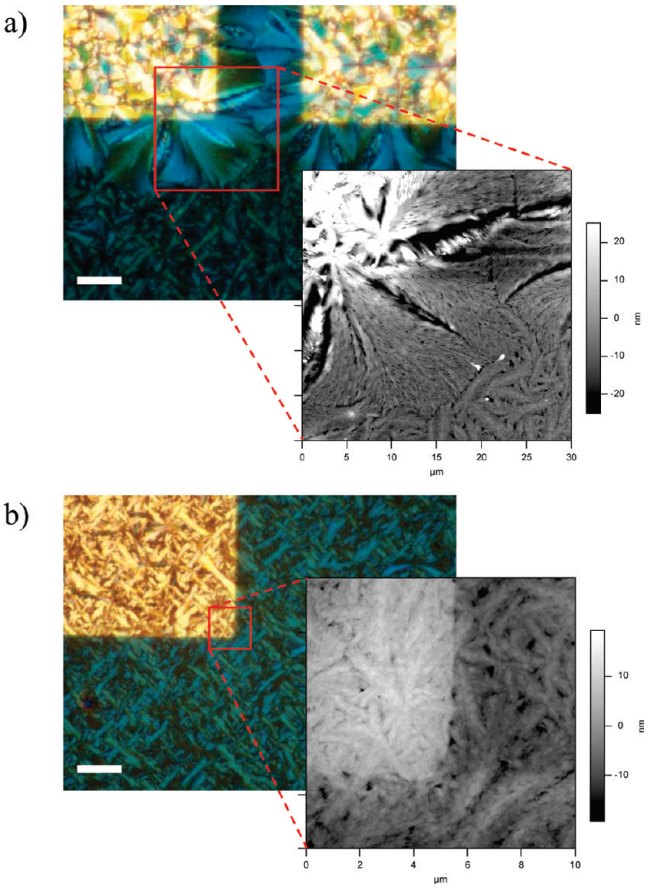

Figure 5. Cross-polarized optical and AFM images of DiF-TESADT TFTs on (a) PFBT-treated electrodes of TFT with L = 20 μm and (b) untreated electrodes of TFT with L = 80 μm. Images of the PFBT-treated electrodes show substantial growth of electrode-nucleated crystals into the TFT channel. Images of untreated electrodes show identical structures on both the oxide and the electrode. Scale bars on optical images are 10 μm. Larger scale AFM images of blanket films can be found in the Supporting Information.

determine the IR transition dipole orientation for both the *syn* and *anti* forms of the molecule, which indicate that an adequate number of strong modes have transition dipoles along the molecule coordinates for both forms to perform an orientation analysis. These lines are indicated in Figure 5 and summarized in Table 1. The primary differences between the two RAIR spectra and the reference lie in the intensity of the out-of-plane C═C−H wagging modes near 870 cm^{-1}. These lines are nearly absent on PFBT-treated Au, indicating an edge-on orientation. They are much stronger on untreated Au, suggestive of a more face-on orientation. The results of the quantitative orientation analysis are reported in Table 2. The orientation distribution average is reported as a single, effective angle, assuming a delta function distribution. An isotropic distribution would thus be reported as the magic angle: 54.7°.

For films on dielectric substrates (such as the untreated oxide), an alternate approach to the orientation analysis can be performed, based on the observed ratio of line intensities in *p*- and *s*-polarized transmission spectra.[34] This approach provides orientation information independent of the assumption of C_{2v} symmetry. The results of such an analysis to transmission spectra (data in Supporting Information) is included in Table 2. The excellent agreement in the effective orientation angles for untrea-

Table 1. Vibrational Mode Frequencies and Assignments for Features Used in the Orientation Analysis

experiment [cm^{-1}]	theory (syn, anti) [cm^{-1}]	assignment	dipole orientation
801	(797, 796)	C═CH op[a] wag	X'
863	(873, 872)	C═CH op wag	X'
870	(884, 882)	C═CH op wag	X'
1364	(1348, 1348)	C6 C═C + C−C	Y'
1403	(1405,-)	C═CH ip[b] bend	Z'
1413	(-,1416)	C═CH ip bend	Z'
1588	(1585, 1586)	C═CF stretch	Z'
2134	(2116, 2115)	C≡C stretch	Y'

[a] op: out-of-plane. [b] ip: in-plane.

Table 2. Summary of Extracted Average Orientation Angles from IR Absorption Studies

Degree (deg)	PFBT	PClBT	UnTr Au	UnTr Oxide	(001)	(111)
θ	69.3 ± 0.4[a]	69.5 ± 0.8	67 ± 1.	64.[b]	71.	69.
ψ	75.8 ± 0.4	75.7 ± 0.9	49. ± 5.	46.	72.	10.
$f_{(001)}$	1.0 ± 0.04	1.0 ± 0.04	0.61 ± 0.09	0.55		

[a] All uncertainties are one estimated standard deviation based upon two or three independently prepared and analyzed films. [b] Uncertainty is expected to be similar to the results on Au.

ted Au and untreated oxide validate the assumptions in the analysis of the RAIRS.

The effective orientation angles are the result of an average over all molecules in the film. If we assume that the film consists entirely of either (00 L) or (111) oriented domains, as identified by GIXD and TEM, we can use the observed average orientation to calculate the volume fraction, *f*, of the (001) domains. Shown in Table 2 are the predicted molecular orientations for the (001) and (111) crystal orientations, based on the high temperature polymorph crystal structure. The estimated (001) volume fraction is also summarized in Table 2. For the PFBT and PClBT-treated films, we find comprehensive (100) orientation within the precision of the measurement. For the untreated Au and oxide substrates, we find comparable amounts of both the (001) and the (111) orientations.

Spatially-Resolved Measurements on Individual Devices. The previous section discussed the microstructure in blanket films of DiF-TESADT deposited on treated and untreated substrates. These measurements reflect the structure of the film on the Au electrodes and the oxide in the field of the devices, but do not provide a measurement of the crystals present in the channels of transistor devices that extend from the gold electrodes onto the oxide. As shown previously, films spin-cast on patterned PFBT-treated Au electrodes have crystals that extend beyond the edges of the electrode into the transistor channel.[26,37] This structure is critical to the transistor performance, as long channel devices where the edge-grown crystals do not bridge the transistor channel have substantially lower charge carrier mobility. Additionally, transistors with untreated electrodes have substantially lower charge carrier mobility and show no effects of the electrodes on the film microstructure. Figure 5 shows polarized optical micrographs and corresponding AFM images of the channels of PFBT-treated and untreated electrodes. The polarized optical micrographs show that the platelet-like crystals on the PFBT-treated electrodes extend out over the oxide channel region with a fan-like growth front. The birefringence of the crystals shows a common orientation in each of the growth front fans. The crystallographic orientation of these crystals will be examined later by electron diffraction. These platelet-like regions can be followed back to the crystal on the electrode where they originated. The AFM image provides a higher resolution image of the crystals growing out from the electrode. The AFM image and the optical image also show the much finer structure in the field of the oxide away from the electrode edge. This same microstructure is observed to cover uniformly both the untreated electrodes and the oxide in Figure 5b. For untreated electrodes, the microstructure of the DiF-TESADT film is independent of the substrate surface (consistent with the blanket film studies) and continuous across the electrode step edge. The AFM image only identifies the electrode edge because of the change in height. Similarly the optical micrograph only identifies the electrode because of the change in optical reflectivity between the silicon oxide and the Au electrode.

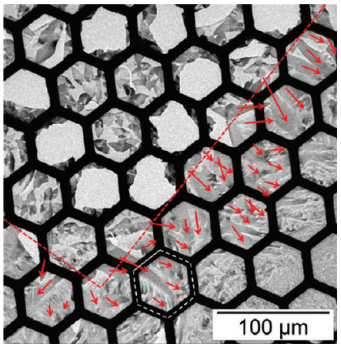

Figure 6. TEM image showing the microstructure of a delaminated film from an electrode edge on PFBT-treated device. The red dashed line denotes the edge of the former electrode. Red arrows were obtained from selective area diffraction measurements and denote the orientation of the (010) planes. White hexagon denotes the region investigated in Figure 7.

The microstructure of the film and the local crystal orientation were further investigated with TEM analysis of a film delami-

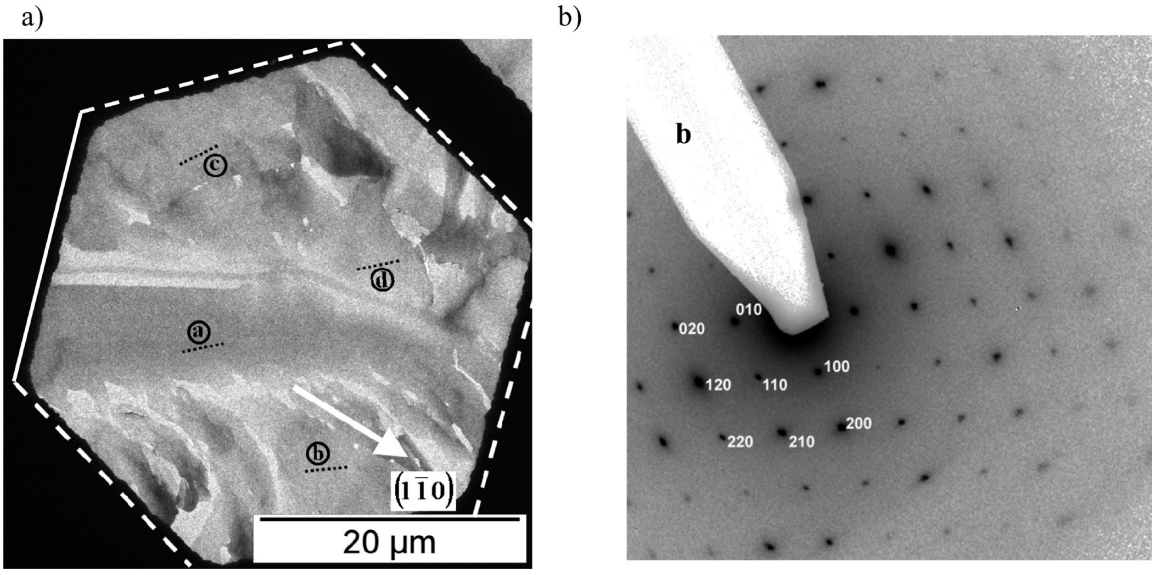

Figure 7. Crystal branches at the transition between the two crystal habits. (a) TEM image of the region highlighted by the white lines in Figure 6. The lines have been retained here to indicate the orientation of this image in relation to Figure 6. The black dotted lines indicate the local (010) orientation. The region labeled **a** is a part of the main crystal lath that extends from the treated electrode (out of view to the left). This crystal has numerous branches that protrude along the $[1\bar{1}0]$ direction toward the lower half of the figure. (b) The corresponding electron diffraction of the region labeled **b** in (a), shown in the same orientation.

nated from a transistor device. Selective area electron diffraction was conducted at a series of positions near the electrode edge and showed a preferential orientation of the nominally (010) planes radiating away from the electrode edge (Figure 6). This result is consistent with a (010) primary growth face for the platelets. Fast in-plane growth along the (010) face is supported by the shape anisotropy of the platelets on the treated contacts, and the single crystal habit for vapor phase growth.[38] On treated contacts the anisotropy is not remarkable, because crystals continue to grow in other directions after initial impingement. The platelet shape is thus merely oblong with the longest axis approximately the (010). This direction also is transverse to the π-planes and therefore is expected to have the high charge transport because of the strong intermolecular coupling between adjacent molecular cores. This preferential orientation of the (010) planes, and thus the π-planes, perpendicular to the electrodes and across the conducting channel should result in a large charge carrier mobility. While these large lath-shaped crystals owe their shape to crystal growth kinetics, their large size is governed by nucleation kinetics: crystals nucleate earlier during the drying process on the treated electrode surface and therefore can extend further over the untreated surface before impinging with the relatively slower nucleating aggregates there. Note that these edge-nucleated crystals form on the surface of the electrode near the edge, and not on the actual step edge. They nucleate with a random azimuthal orientation, just as those far from the edge. Those with (010) at a shallow angle to the electrode edge impinge with neighbors early and do not grow to as great length as those oriented approximately perpendicular to the edge.

Next, we examine how the (001) crystal habit, which is stable on the treated surfaces, exhibits a crystal habit transformation on untreated surfaces. This transformation occurs through crystal branching along the $(1\bar{1}0)$ plane (Figure 7). These crystal branches nucleate on the lateral surfaces of the lath especially and eventually the (010) face itself. They commence away from the lath in the $[1\bar{1}0]$direction, and as they proceed curve slightly. These branches retain mainly the (001) out-of-plane orientation of the parent lath.

Figure 8 shows TEM images and selective area diffraction of the DiF-TESADT microstructure on the untreated oxide as is the case for the field regions away from the electrode edges. The fan-like microstructure has a preferred in-plane orientation despite consisting of a fine scale mixture of the (111) and (001) phases. Electron diffraction shows that the (111) and (001) oriented crystals locally share a common plane of $(1\bar{1}0)$, and thus the fine rod-like crystals are homoepitaxially related. Angular relationships between these crystals and diffraction from region (d) highlighted in Figure 8 suggest twinning about the (010). The aggregates exhibit a bow-tie appearance with the $(1\bar{1}0)$ extending toward the corners of the aggregate. The $[1\bar{1}0]$ direction is thus the primary growth direction observed in the mixed phase structure, which at least on the untreated surfaces is faster than the (010). This relative slowness of the (010) here may be associated with poisoning by homoepitaxy. As noted before (Figure 3), molecules lie approximately flat on the substrate in the (111) crystal orientation, suggesting that surface adsorption influences the crystal growth kinetics here.

DISCUSSION

The excellent crystal forming characteristics of diF-TESADT enable high mobilities within the *a*-*b* plane of single grains, while the mixed phase films formed on untreated surfaces have poor electrical performance. The ability to create highly textured device channels by proper treatment of the contact allows exceptional device performance from spin coated films.[26] Microscopy and diffraction measurements establish the microscopic origin of the self-patterning during the film drying process. PFBT-treated electrodes produce (001) platelets with their fast growth and the preferred charge transport axes in the plane of the film (and the plane of charge transport in TFTs). On untreated electrodes and the oxide dielectric, the polycrystalline structure consists of alternating rod-like crystals with (001) and (111) orientations,

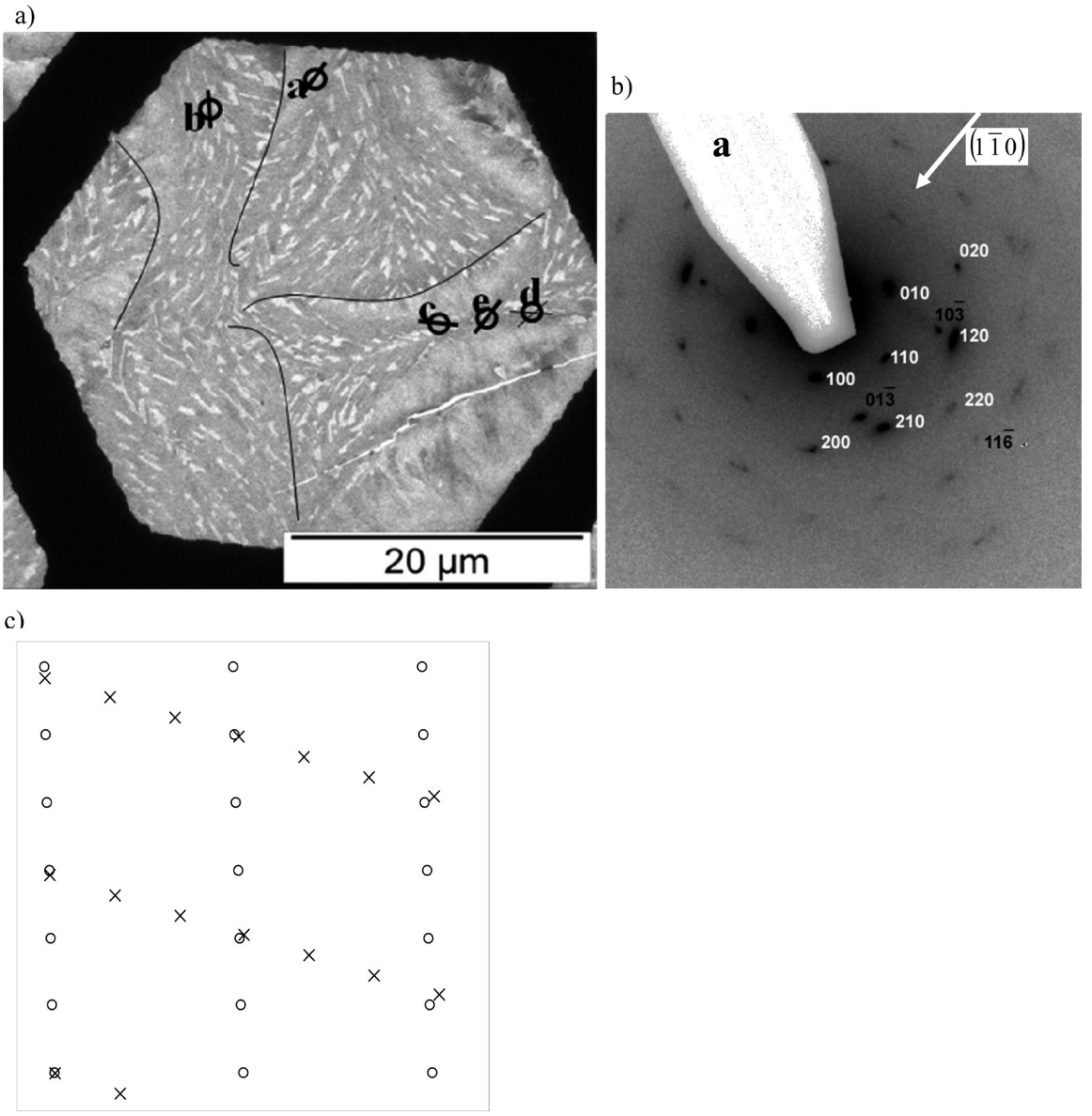

Figure 8. TEM Image of a film on untreated oxide showing structure of mixed phase present in the field of the TFTs. This structure comprises bow-tie aggregates, whose boundaries are marked with thin lines. Several sites on the field are marked with a letter and the $[1\bar{1}0]$ direction, which points roughly toward the corners of the aggregate. (Note that for this crystal structure, the plane normal of the $(1\bar{1}0)$ and the direction $[1\bar{1}0]$ are nearly parallel, differing by only 2.2°.) (b) Electron diffraction from the region marked (a), which shows a mixture of the (001) and (111) orientations. These two phases share a common $(1\bar{1}0)$ plane in the plane of the film. (c) Plot of the reciprocal lattice nets in the $[1\bar{1}0]$ zone for the (001) and (111) orientations, denoted by **o** and **x** respectively. The lattice nets are rotated by 71.5°.

that is, tilted at 71° relative to one another, separated by narrow bands rich in (001) oriented platelets. For the (111) orientation, the (010) growth direction (and the preferred charge transport direction) are oriented out of plane at 32° above the horizon (see Figure 9). The common plane, $(1\bar{1}0)$, observed between the (111) and (001) crystal orientations is likely a secondary growth face. The much faster growth of the (010) face of the (001) platelets on PFBT-treated Au is in the plane of the film and allows each nucleated platelet to grow considerable distances before impinging on a neighboring platelet. The (111) oriented platelets, on the other hand, can grow along the (010) face only until the growth face reaches the film surface and then growth is limited by large-scale diffusion of new molecules to the growth front. Once this occurs, the crystals on untreated surfaces grow predominantly along the $[1\bar{1}0]$ direction.

The large crystal laths that grow out away from the electrode over the untreated surface indicate that the (001) is stable for a time and only eventually is disrupted by homoepitaxy. If the primary nucleation event on the field that marks the center of the crystal aggregate there were of the (001) orientation, we would therefore expect that the (001) would persist some distance. However, the two orientations are mixed at the very center, and the fine rod-shaped crystals characteristic of the (111) orientation are observed there. Therefore, we suggest that the primary nucleation event is in the (111) orientation, as would be favored by face-on adsorption of molecules to the untreated substrate.

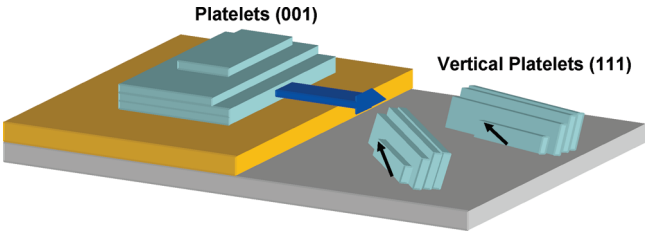

Figure 9. Model for growth showing formation of lying down platelets on treated Au and a mixture of vertical platelets and small lying down platelets on the untreated oxide. The platelets on the edge of the electrodes extend into the oxide region. The (010) growth direction is denoted with the arrows.

The (001) orientation may then nucleate by homoepitaxy, but it is not able to overtake the (111), which is always present.

For the heterogeneous structure of patterned electrodes that have been treated with PFBT, platelets that nucleate near an electrode edge with their (010) growth face oriented toward the oxide region grow over the neighboring oxide regions. For these edge-nucleated crystals to grow over the oxide without impingement, either the nucleation on PFBT-treated surfaces during film drying is faster than on untreated surfaces or the small crystals present in the untreated oxide are consumed by the growing platelet in an Oswald ripening process. For transistors with sufficiently narrow channels, the (010) growth fronts from adjacent electrodes bridge the channel and provide a high mobility path for the charge carriers to cross the channel.

It is interesting to speculate on the origin of the substrate control over crystal orientation. The vapor growth of (001) oriented platelet single crystals on both glass plates[6] and untreated Au (Supporting Information) suggests that the low energy crystal habit is (001) oriented and the mixed (111) and (001) film is the result of kinetic constraints during the rapid film formation during sample drying. Simple free energy considerations suggest that a face-on (111) orientation would be favored on polarizable surfaces such as untreated Au and (001) platelets would be favored on a low energy surface.[39,40] Vapor deposited thin film of pentacene have been extensively studied as models for the organization of surface-confined molecular crystals. Deposition of pentacene on low to moderate (OTS-treated or clean silica) free energy surfaces results in the formation of a monolayer phase, with a virtually upright molecule.[41] Further deposition results in the formation of a distinct thin film phase with a vertical *d*-spacing typically 15.4 Å versus the bulk 14.5 Å,[42,43] which ultimately breaks-up into the bulk phase. Deposition of pentacene on non-reactive clean metals such as Au, Ag, and Cu, typically results in a "laying down" monolayer phase, consistent with maximal overlap between the π system of the pentacene molecule and the free electrons of the metal.[39,40] The presence of a SAM layer of either polar or nonpolar character inhibits the formation of the face-on monolayer, and the near upright thin film phase is typically reported.[44,45] Significant contact effects in TFTs have been attributed to the presence of the face-on orientation on untreated Au contacts.[46]

It has been hypothesized that PFBT specifically orients the molecules into a (001) motif because of S−F interactions similar to those that support the crystallization of the material.[26] However, PFBT also significantly lowers the surface energy (water contact angle is ≈88°) and could act solely by "passivating" the high energy interfaces. PClBT results in a similar low surface energy (water contact angle is ≈72°) and also inhibits the (111) orientation. BT films, with identical water contact angle to PClBT (Supporting Information) do not fully suppress the (111) orientation, as evidenced in the electrical performance and diffraction measurements (Supporting Information). Thus it appears that surface energy alone is not the origin of the influence of PFBT and PClBT on DiF-TESADT orientation, and that the halogen-chalcogen interaction likely is important.

CONCLUSION

We have used a combination of microscopy, spectroscopy, and diffraction to determine the dependence of DiF-TESADT microstructure on the substrate chemistry and identified the mechanisms for self-patterning responsible for the high mobility of DiF-TESADT spin-cast films and for highly insulating portions of these films that adopt a different morphology. We have found that PFBT-treated Au surfaces preferentially form large (001) oriented platelets of DiF-TESADT, while untreated Au and untreated oxide form a finely mixed film of (001) and (111) oriented crystals. Molecular adsorption onto the substrate therefore influences the growth habits and growth habit transformations. For patterned Au, platelets nucleated near the edge of the electrode grow unimpinged into the transistor channel over the untreated oxide. The growth into the channel occurs along the (010) growth face, the direction of high charge transport, resulting in a substantially enhanced charge carrier mobility when growth fronts from adjacent electrodes meet.

ASSOCIATED CONTENT

Supporting Information. Water contact angle, ellipsometry, RAIRS, and XPS characterization of the PFBT, PClBT, and BT SAMs. Brewster angle, polarized transmission IR spectra of the DiF-TESADT films on untreated oxide substrates. Optical microscopy of (001) platelets grown on untreated Au in a vapor oven. Transmission electron microscopy and atomic force microscopy of blanket films on treated and untreated surfaces. GIXD measurements of films on PClBT and BT-treated substrates. This material is available free of charge via the Internet at http://pubs.acs.org.

AUTHOR INFORMATION

Corresponding Author

*E-mail: joe.kline@nist.gov (R.J.K.), lee.richter@nist.gov (L.J.R.).

ACKNOWLEDGMENT

Portions of this research were carried out at the Stanford Synchrotron Radiation Laboratory, a national user facility operated by Stanford University on behalf of the U.S. Department of Energy, Office of Basic Energy Sciences. J.E.A. and S.S. acknowledge the Office of Naval Research for support. We thank Christina Hacker for the XPS measurements of the SAM films.

REFERENCES

(1) Arias, A. C.; Mackenzie, J. D.; Mcculloch, I.; Rivnay, J.; Salleo, A. *Chem. Rev.* **2010**, *110* (1), 3–24.
(2) Horowitz, G. *J. Mater. Res.* **2004**, *19* (7), 1946–1962.
(3) Gelinck, G.; Heremans, P.; Nomoto, K.; Anthopoulos, T. D. *Adv. Mater.* **2010**, *22* (34), 3778–3798.

(4) Reese, C.; Bao, Z. N. *Mater. Today* **2007**, *10* (3), 20–27.
(5) De Boer, R. W. I.; Gershenson, M. E.; Morpurgo, A. F.; Podzorov, V. *Phys. Status Solidi A* **2004**, *201* (6), 1302–1331.
(6) Jurchescu, O. D.; Subramanian, S.; Kline, R. J.; Hudson, S. D.; Anthony, J. E.; Jackson, T. N.; Gundlach, D. J. *Chem. Mater.* **2008**, *20* (21), 6733–6737.
(7) Xia, Y.; Kalihari, V.; Frisbie, C. D.; Oh, N. K.; Rogers, J. A. *Appl. Phys. Lett.* **2007**, *90* (16), 162106.
(8) Gershenson, M. E.; Podzorov, V.; Morpurgo, A. F. *Rev. Mod. Phys.* **2006**, *78* (3), 973.
(9) Briseno, A. L.; Mannsfeld, S. C. B.; Ling, M. M.; Liu, S.; Tseng, R. J.; Reese, C.; Roberts, M. E.; Yang, Y.; Wudl, F.; Bao, Z. *Nature* **2006**, *444* (7121), 913–917.
(10) Gundlach, D. J.; Lin, Y. Y.; Jackson, T. N.; Nelson, S. F.; Scholm, D. G. *IEEE Electron Device Lett.* **1997**, *18* (3), 87–9.
(11) Merlo, J. A.; Newman, C. R.; Gerlach, C. P.; Kelley, T. W.; Muyres, D. V.; Fritz, S. E.; Toney, M. F.; Frisbie, C. D. *J. Am. Chem. Soc.* **2005**, *127* (11), 3997–4009.
(12) Klauk, H. *Chem. Soc. Rev.* **2010**, *39* (7), 2643–2666.
(13) Mcculloch, I.; Heeney, M.; Chabinyc, M. L.; Delongchamp, D.; Kline, R. J.; Coelle, M.; Duffy, W.; Fischer, D.; Gundlach, D.; Hamadani, B.; Hamilton, R.; Richter, L.; Salleo, A.; Shkunov, M.; Sporrowe, D.; Tierney, S.; Zhong, W. *Adv. Mater.* **2009**, *21* (10−11), 1091–1109.
(14) Sirringhaus, H.; Ando, M. *MRS Bull.* **2008**, *33* (7), 676–682.
(15) Osaka, I.; Mccullough, R. D. *Acc. Chem. Res.* **2008**, *41* (9), 1202–1214.
(16) Anthony, J. E. *Chem. Rev.* **2006**, *106* (12), 5028–5048.
(17) Murphy, A. R.; Frechet, J. M. J. *Chem. Rev.* **2007**, *107* (4), 1066–1096.
(18) Afzali, A.; Dimitrakopoulos, C.; Breen, T. *J. Am. Chem. Soc.* **2002**, *124* (30), 8812–8813.
(19) Anthony, J. E.; Brooks, J. S.; Eaton, D. L.; Parkin, S. R. *J. Am. Chem. Soc.* **2001**, *123*, 9482–3.
(20) Hamilton, R.; Smith, J.; Ogier, S.; Heeney, M.; Anthony, J. E.; Mcculloch, I.; Veres, J.; Bradley, D. D. C.; Anthopoulos, T. D. *Adv. Mater.* **2009**, *21* (10−11), 1166–1171.
(21) Kang, J.; Shin, N.; Jang, D. Y.; Prabhu, V. M.; Yoon, D. Y. *J. Am. Chem. Soc.* **2008**, *130* (37), 12273–12275.
(22) Dickey, K. C.; Anthony, J. E.; Loo, Y. L. *Adv. Mater.* **2006**, *18* (13), 1721–1726.
(23) Lee, S. S.; Kim, C. S.; Gomez, E. D.; Purushothaman, B.; Toney, M. F.; Wang, C.; Hexemer, A.; Anthony, J. E.; Loo, Y. L. *Adv. Mater.* **2009**, *21* (35), 3605–3609.
(24) Reichenbacher, K.; Suss, H. I.; Hulliger, J. *Chem. Soc. Rev.* **2005**, *34* (1), 22–30.
(25) Subramanian, S.; Park, S. K.; Parkin, S. R.; Podzorov, V.; Jackson, T. N.; Anthony, J. E. *J. Am. Chem. Soc.* **2008**, *130* (9), 2706–2707.
(26) Gundlach, D. J.; Royer, J. E.; Park, S. K.; Subramanian, S.; Jurchescu, O. D.; Hamadani, B. H.; Moad, A. J.; Kline, R. J.; Teague, L. C.; Kirillov, O.; Richter, C. A.; Kushmerick, J. G.; Richter, L. J.; Parkin, S. R.; Jackson, T. N.; Anthony, J. E. *Nat. Mater.* **2008**, *7* (3), 216–221.
(27) Jurchescu, O. D.; Hamadani, B. H.; Xiong, H. D.; Park, S. K.; Subramanian, S.; Zimmerman, N. M.; Anthony, J. E.; Jackson, T. N.; Gundlach, D. J., . *Appl. Phys. Lett.* **2008**, *92*, (13).
(28) Park, S. K.; Mourey, D. A.; Subramanian, S.; Anthony, J. E.; Jackson, T. N. *Appl. Phys. Lett.* **2008**, *93* (4), 043301.
(29) Park, S. K.; Mourey, D. A.; Subramanian, S.; Anthony, J. E.; Jackson, T. N. *Adv. Mater.* **2008**, *20* (21), 4145–4147.
(30) Smith, J.; Hamilton, R.; Qi, Y.; Kahn, A.; Bradley, D. D. C.; Heeney, M.; Mcculloch, I.; Anthopoulos, T. D. *Adv. Funct. Mater.* **2010**, *20* (14), 2330–2337.
(31) Jurchescu, O. D.; Mourey, D. A.; Subramanian, S.; Parkin, S. R.; Vogel, B. M.; Anthony, J. E.; Jackson, T. N.; Gundlach, D. J. *Phys. Rev. B* **2009**, *80* (8), 085201.
(32) Certain commercial equipment, instruments, or materials are identified in this paper to specify the experimental procedure adequately. Such identification is not intended to imply recommendation or endorsement by the National Institute of Standards and Technology, nor is it intended to imply that the materials or equipment identified are necessarily the best available for the purpose.
(33) Chabinyc, M. L.; Toney, M. F.; Kline, R. J.; Mcculloch, I.; Heeney, M. *J. Am. Chem. Soc.* **2007**, *129* (11), 3226–3237.
(34) Gurau, M. C.; Delongchamp, D. M.; Vogel, B. M.; Lin, E. K.; Fischer, D. A.; Sambasivan, S.; Richter, L. J. *Langmuir* **2007**, *23* (2), 834–842.
(35) Hacker, C. A.; Batteas, J. D.; Garno, J. C.; Marquez, M.; Richter, C. A.; Richter, L. J.; Van Zee, R. D.; Zangmeister, C. D. *Langmuir* **2004**, *20* (15), 6195–6205.
(36) Kang, J. F.; Ulman, A.; Liao, S.; Jordan, R. *Langmuir* **1999**, *15* (6), 2095–2098.
(37) Teague, L. C.; Hamadani, B. H.; Jurchescu, O. D.; Subramanian, S.; Anthony, J. E.; Jackson, T. N.; Richter, C. A.; Gundlach, D. J.; Kushmerick, J. G. *Adv. Mater.* **2008**, *20* (23), 4513–4516.
(38) Jurchescu, O. D.; Subramanian, S.; Kline, R. J.; Hudson, S. D.; Anthony, J. E.; Jackson, T. N.; Gundlach, D. J. *Chem. Mater.* **2008**, *20* (21), 6733–6737.
(39) Kang, J. H.; Zhu, X. Y. *Appl. Phys. Lett.* **2003**, *82* (19), 3248–3250.
(40) Sohnchen, S.; Lukas, S.; Witte, G. *J. Chem. Phys.* **2004**, *121* (1), 525–534.
(41) Fritz, S. E.; Martin, S. M.; Frisbie, C. D.; Ward, M. D.; Toney, M. F. *J. Am. Chem. Soc.* **2004**, *126* (13), 4084–4085.
(42) Dimitrakopoulos, C. D.; Malenfant, P. R. L. *Adv. Mater.* **2002**, *14* (2), 99–117.
(43) Mannsfeld, S. C. B.; Virkar, A.; Reese, C.; Toney, M. F.; Bao, Z. N. *Adv. Mater.* **2009**, *21* (22), 2294–2298.
(44) Hu, W. S.; Tao, Y. T.; Hsu, Y. J.; Wei, D. H.; Wu, Y. S. *Langmuir* **2005**, *21* (6), 2260–2266.
(45) Auml; Fer, D.; Ruppel, L.; Witte, G. *Phys. Rev. B* **2007**, *75* (8), 085309.
(46) Lee, K. S.; Smith, T. J.; Dickey, K. C.; Yoo, J. E.; Stevenson, K. J.; Loo, Y. L. *Adv. Funct. Mater.* **2006**, *16* (18), 2409–2414.